Tenth International Conference on Computational Fluid Dynamics (ICCFD10), Barcelona, Spain, July 9-13, 2018

ICCFD10-2018-015

A Flow Feature Extraction Method for Shock-Fitting Computation

Zedong Chen*, Dongyang Zou*, Fan Zhang** and Jun Liu*
Corresponding author: chenzd_dut@163.com

* State Key Laboratory of Structural Analysis for Industrial Equipment, Dalian University of Technology, Dalian 116024, China.
** School of Aeronautics and Astronautics, Sun Yat-sen University, Guangzhou 510006, China.

Abstract: We present a surface extraction method named Point-Rays method to model the geometry of shock waves or contact discontinuities for the shock-fitting computation. While using this method, a bunch of grid vertexes will be detected and marked as a point set by shock detection procedures that work on the flow field results. Then, the discrete point set will be divided into several subsets by a series of rays for piecewise fitting. Finally, a continuous smooth surface can be reconstructed based on the piecewise-fitted fragments. This algorithm is also extended to three-dimensional applications by introducing an unit-sphere model. The present method shows a new path to provide the initial surface of discontinuities for shock-fitting, especially in complex 3D problems. Computations show that the converged solution will be obtained within a few time steps with using this method. This method is also expected to be used in adaptive mesh refinement procedures.

Keywords: Supersonic flows, Shock-detection, Shock-Fitting, Surface fitting.

1 Introduction

It is well known that shock wave is a highly nonlinear phenomenon in aerodynamics and gas dynamics. Initially Computational Fluid Dynamics (CFD) was unable to simulate this phenomenon until Lax [1, 2] proposed weak solutions of nonlinear hyperbolic equations in 1954. Then many shock-capturing schemes such as TVD [3], NND [4], ENO [5], and WENO [6] were presented to capture complex shock waves. Although the property of shock wave is taken into account in designing shock-capturing schemes, in essence it is similar to von Neumann's idea [7] which describes the discontinuity as a transition region where the flow field continuously changes. In other word, the numerical shock wave in shock-capturing simulations is not a real discontinuity.

A CFD solution is an approximation to partial differential equations, and thus it can only present the flow phenomena that are described by the equations, in theory, which is why the compatibility so important. The Navier-Stokes equations are based on Stokes hypothesis ($3\lambda + 2\mu = 0$, where λ is volumetric expansion coefficient, and μ is dynamic viscosity. However, this hypothesis is not valid on shock waves [8] where there are non-equilibrium thermodynamic processes inside and large change in the flow velocity. Therefore, the researchers of rarefied gas dynamics believe that "In theory, the Navier-Stokes equations cannot be used to describe shock structures" [9]. In the theory of inviscid flow, shock waves will be considered as discontinuities, and the flow variables on both sides of the discontinuity satisfy the Rankine-Hugoniot (R-H) relation.

Theoretically, a discontinuity has two sets of variables at the same spatial position, on each side of the discontinuity. Moreover, there are four sets of variables at the triple point of Mach reflection. Therefore, it is impossible to obtain a true discontinuity by describing the shock wave with the continuous change of flow field, and the numerical solution has no physical meaning in the transition region, i.e. the numerical shock wave. Moreover, it is also impossible to evaluate the accuracy of the shock-capturing schemes in the numerical shock waves.

In the 1960s, Moretti et al. developed a shock-fittting technique which produced the numerical solution of supersonic blunt body flow on a CDC 6600 computer in only 6 minutes [10]. In 2002, Moretti reviewed the progress of shock simulation over the past 36 years, compared the results of shock-capturing schemes and the shock-fitting schemes for the supersonic blunt body flow, and concluded that the shock-fitting schemes should be developed for accurately simulating shock waves [11]. Zhang's [12] evaluation of shock-fitting method in 2010 is typical: "The shock-fitting method has the advantages of high calculation accuracy and clear physical concepts, but the calculation process is complicated and the calculation cost is large and the approximate location of the shock wave should be predictable. In general, the shock-fitting method is only applicable to the steady flows where the shock wave structure is relatively simple and the shock wave shape and position can be estimated in advance."

The motion and deformation of shock waves in the calculation process make the application of the shock-fitting method more complicated. Although usually the shock-fitting method requires fewer grid cells, it has to deal with the mapping between the discrete shock points and grid vertexes, which greatly increases the complexity. The earliest shock-fitting technique proposed by Moretti is a realization of "boundary-shock", which needs to partition the flow field and can only deal with the detached shock with relatively regular shape and small displacement. In 1967, Richtmyer et al. [13] proposed a floating shock-fitting method allowing the fitted shock wave to float on the background mesh. This method was later used to simulate internal shock waves [14]. Zhong et al. [15,16] associated this method with a high-order finite-difference scheme to effectively improve the accuracy in simulating the internal smooth flow field, and the method was successfully applied to the solution of many hypersonic flows. Paciorri and Bonfigolioli et al. [17, 18] presented a shock-fitting technique for unstructured grids to overcome the topological limitations of structural grids. This method requires recording the location of the shock front over the background mesh and the local re-meshing, which inevitably leads to the requirement of interpolation between the original grid and the re-meshed grid. In 2015, Liu et al. [19] presented a moving discontinuity-fitting method with unstructured dynamic mesh based on the arbitrary Lagrange-Euler method. In Liu's method, the discontinuity surface is represented by a series of mesh grid vertexes, its motion is driven by the R-H relations. Then, the new positions of other vertexes are determined by an unstructured dynamic grid technique [20] based on both linear and torsional spring analogies. Compared with the Paciorri and Bonfigolioli's method, Liu's method does not require the reconstruction of the mesh during each step, so that the interpolation errors can be avoided and parallel computation is easier to be implemented. Regular reflections and Mach reflections were simulated with this method in [21–23].

In order to improve the flexibility of shock-fitting method, we present a solution of flow feature extraction. This method can automatically fit shock wave surfaces captured by shock-capturing methods and replaces Riemann solvers with the R-H relations on the shock wave surfaces.

At present, there are mainly three types of commonly used shock detection algorithms. The first method determines the shock surface based on the maximum variable gradient [24]. This method is simple to implement, but it is necessary to set some appropriate filters to eliminate false results. The second method is the normal Mach number method [25]. This method assumes the Mach number normal to a shock surface is equal to 1. It is more adaptable than the first one, but it also requires an appropriate filter and is difficult to detect contact discontinuities. The third method is based on the theory of characteristics [26, 27]. This method is more accurate and more effective than the previous two methods, but the implementation process is complicated and the cost of calculation is large. The shock wave identified by the above algorithms is usually a shock band of certain width, which is difficult to be directly used in shock-fitting method, especially for complex three-dimensional problems. Therefore, it is necessary to develop a new algorithm to promote the practical application of shock-fitting method.

In this paper, we present a surface extraction method named Point-Rays (PRs) method to model the geometry of shock waves or contact discontinuities. This method can fit the shock wave band in the flow field, into a continuous smooth surface. This surface can be used as the shock surface in shock-fitting method. In section 3, two-dimensional calculation process is introduced in detail, and then the extension to three-dimension is briefly introduced. The numerical results are listed in section 4.

2 Flow feature detection

We have developed a shock-fitting method on unstructured dynamic meshes [19, 21–23], where the shock-capturing method is used to obtain an initial flow field, and then the shock wave detector is used to identify and locate the shock wave in the flow field to embed the R-H relations. Because shock vertexes coincide with mesh grid vertexes, the description of shock motions can be easily implemented using dynamic mesh techniques. The shock speed is determined by solving R-H relations. In this paper, the main discontinuities are fitted with the R-H relations, other regions are simulated with the shock-capturing method, so it is a fitting-capturing hybrid procedure.

In order to fit the shock wave, its location should be determined at first. The three aforementioned shock detection methods are commonly used. Considering that we need to identify both the shock waves and the contact discontinuities, a simple gradient-based detector is used, which is defined at each element as follows:

$$\begin{aligned} k_p &= \frac{|\nabla p|}{|\nabla p|_{\max}}, \\ k_\rho &= \frac{|\nabla \rho|}{|\nabla \rho|_{\max}} \end{aligned} \tag{1}$$

where k is the gradient ratio, and the subscript *max* represents the maximum value of the gradient of the flow field variables.

- For shock waves detection: Considering that the pressure gradient and the density gradient on the shock wave are much larger than that on the uniform flow, we set a pressure or density threshold factor, i.e. $k^s_{\text{thre},p}$ or $k^s_{\text{thre},\rho}$, and shock wave will be detected by satisfying $k_p > k^s_{\text{thre},p}$ or $k_\rho > k^s_{\text{thre},\rho}$.
- For contact discontinuities detection: Considering that the density on the two sides of a contact discontinuity surface varies greatly, but the pressure is equal, we set a pressure threshold factor $k^c_{\text{thre},p}$ and a density threshold factor $k^c_{\text{thre},\rho}$, and contact discontinuities will be detected by satisfying $k_p < k^c_{\text{thre},p}$ and $k_\rho > k^c_{\text{thre},\rho}$.

It is noticed that the threshold factor is an empirical parameter which needs to be adjusted according to different flow conditions, but in this paper we will not paid much attention on this issue.

3 Flow feature extraction method

3.1 Extraction process in 2D

In this section, we present the PRs method for extracting flow field features in two-dimensional cases. The shock wave or contact discontinuity surfaces will be obtained for shock-fitting algorithm based on the following process (also see figure 1):

1. Detect the flow field feature (shock wave or contact discontinuity) with appropriate detectors based on the captured flow field. See figure 1(a).

2. Record and collect the cells based on the flow feature detected in step 1. The vertices or centers of all these cells constitute a point set T. Denote the region of flow feature as A. See figure 1(b).

3. Set source point position and angles. Set a source point S at a appropriate position according to the point set T. Set rays $l_1 \cdots l_i \cdots l_n$ emitted from point S and angles $\varphi_1 \cdots \varphi_i \cdots \varphi_{n-1}$, where n is the number of rays, and φ_i is the angle between ray l_i and ray l_{i+1}. Then, the detected flow field feature region A is divided into $n-1$ subregions $A_1 \cdots A_i \cdots A_{n-1}$ by these rays, and the ray l_i and ray l_{i+1} are the boundaries of subregion A_i. Furthermore, all discrete points in each subregion constitute a subset T_i, and

$$T = \bigcup_{i=1}^{n} T_i \quad \textit{and} \quad T_i \bigcap_{i \neq j} T_j = \emptyset,$$

where $\emptyset$ is an empty set.

4. Adjust source point position and angles. Count the number of points for each subregion $A_i, i = 1, \ldots, n-1$, denoted as N_i. If $N_i < m$, where m is a constant number and usually taken as 3, curve fitting will be not performed in this subregion. If there are adjacent subregions in which each N_i is less than m, the position of the source point or the angles between the rays will be adjusted until the number of discrete points in each subregion is satisfied. This step is to ensure the continuity and smoothness of the fitted curve.

5. Fit a curve in each subregion. A line segment $P_{i,i}P_{i+1,i}$ will be obtained by linearly fitting (e.g. least squares fitting) the subset T_i in subregion A_i, as shown in figure 1(c), where $P_{i,j}$ is the intersection of the straight line fitted in subregion A_j and the ray l_i.

6. Determine the set of feature points. For the inner region, the ray l_i intersects the fitted lines in the regions A_{i-1} and A_i at the points $P_{i,i-1}$ and $P_{i,i}$, respectively. When these two intersections coincide, a point Q_i is called a feature point, and the coordinates satisfy

$$(x_{Q_i}, y_{Q_i}) = (x_{P_{i,i-1}}, y_{P_{i,i-1}}) = (x_{P_{i,i}}, y_{P_{i,i}}).$$

   When these two intersections do not coincide, a feature point Q_i is found on the ray l_i, and the coordinates satisfy

$$(x_{Q_i}, y_{Q_i}) = f(x_{P_{i,i-1}}, y_{P_{i,i-1}}, x_{P_{i,i}}, y_{P_{i,i}}).$$

   In this paper, f is a weight function:

$$f(x_{P_{i,i-1}}, y_{P_{i,i-1}}, x_{P_{i,i}}, y_{P_{i,i}}) = w_{i-1}(x_{P_{i,i-1}}, y_{P_{i,i-1}}) + w_i(x_{P_{i,i}}, y_{P_{i,i}}),$$

   where $w_{i-1} = w_i = 0.5$, and the feature point Q_i is the middle point of the line segment $P_{i,i-1}P_{i,i}$. For the boundaries of region A, the intersection points on ray l_1 and l_n will be the feature points, i.e.

$$(x_{Q_1}, y_{Q_1}) = (x_{P_{1,1}}, y_{P_{1,1}}) \quad \text{and} \quad (x_{Q_n}, y_{Q_n}) = (x_{P_{n,n-1}}, y_{P_{n,n-1}}).$$

   All the feature points $Q_i, i = 1, \ldots, n$ constitute a point set Q, and the connection relation between the points is determined and unique, as shown in figure 1(d).

7. Finally, connect all the points in the set Q into a continuous curve, as shown in figure 1(e).

3.2 Extension to 3D

In this section we briefly introduce the 3D extension of the PRs method. Similar to the two-dimensional process, in 3D, firstly, the detectors are used to obtain a corresponding point set of shock waves and contact discontinuities in the flow field calculated by the shock-capturing method, and then the rays are used to divide the set of points into several subsets, and the points in each subset will be fitted into a triangular patch. Finally, all the triangular patches will be assembled into a complete continuous surface.

For 3D problems, at least three rays are required to determine a single subregion, and the topological relation between each subregion is more complicated. Therefore, a unit-sphere model is introduced in this section to improve the adaptability of the PRs method in 3D problems, as shown in figure 2. The unit-sphere is centered on source point S and the unit length 1 is the radius. The surface of this unit-sphere is meshed onto triangular cells (see figure 2(a)). The three rays (l_i, l_j, l_k) passing through the vertices (A_i, A_j, A_k) of one triangular cell on the unit-sphere from the source point S determine a subregion. In each subregion A_p (where $p = 1, \ldots, n$, and n is the number of surface mesh cells of the unit-sphere), the points will be fitted into a triangular patch $B_{i,p}B_{j,p}B_{k,p}$ (see figure 2(b)). Taking into account the continuity between the triangular patches in adjacent subregions, the position of the intersections on the three rays is adjusted using a method similar to that of the 2D method, and then the final triangular patch $B_iB_jB_k$ in each subregion is determined, see figure 2(c). Therefore, we have obtained a series of triangular patches with continuous vertices, the connection relation of which is the same as that of the unit-sphere mesh, and thus it is easy to assemble them into a continuous surface.

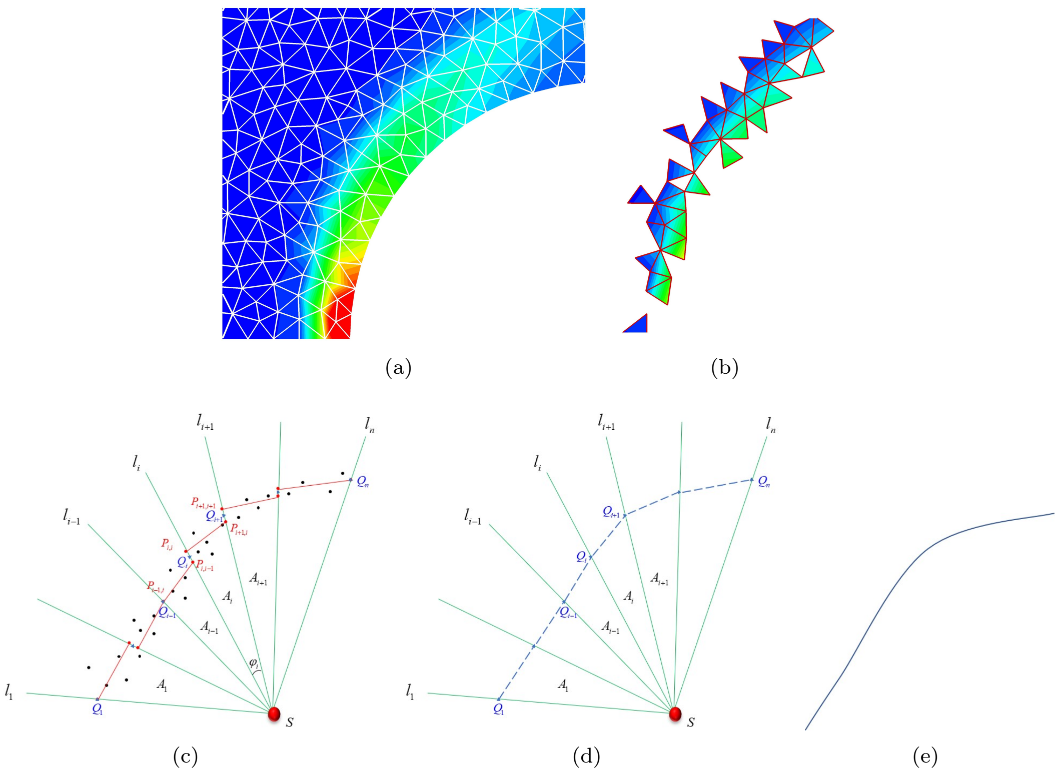

Figure 1: Schematic of 2D PRs method: (a) the captured flow field; (b) the detected shock wave cells; (c) piecewise fitting the point set; (d) line segments fitted by each point subset; (e) continuous smooth curve composed by line segments.

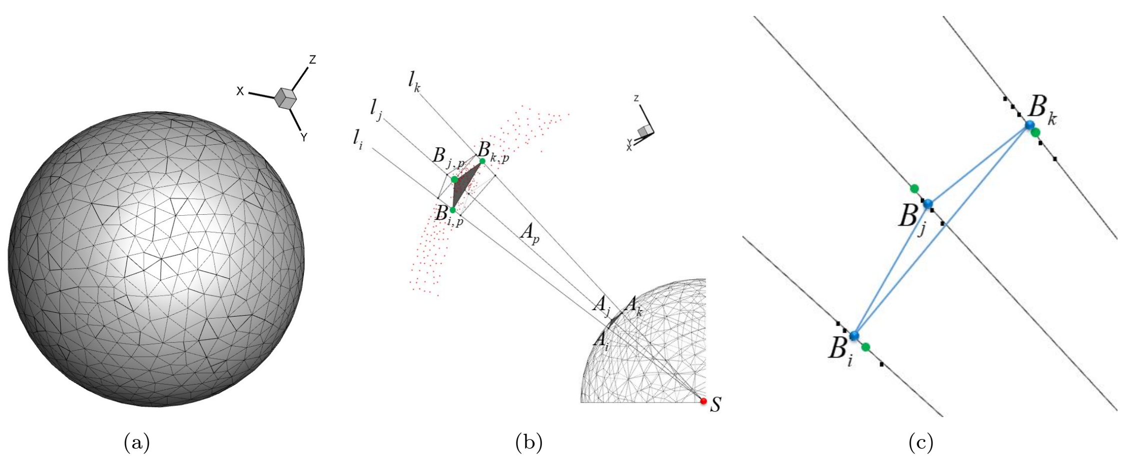

Figure 2: Schematic of 3D PRs method: (a) a unit sphere model; (b) an original triangular patch fitted in a subregion; (c) an adjusted triangle patch (enlarged).

4 Numerical results

4.1 Blunt body problem in 2D

The supersonic blunt body flow has been studied in various researches as a typical detached shock wave problem [28, 29], since it is very challenging for shock-capturing schemes. Here, we also apply it as the primary test case.

In this case, the free-stream Mach number is $Ma = 5.0$, the coordinates of the circular cylinder center is $(0.0, 0.0)$ and the diameter is $D = 0.0508$. The computational grid is 160(circumferential) $\times$ 100(radial), of which the hight of first layer cells is 0.0001, as shown in figure 3(a). At first, the shock-capturing method is used to obtain the flow field structure. The Gauss-Green method is applied to calculate the cell gradient for the second-order spatial discretization, and the MLP-pw limiter [30] is used to improve the stability of calculation. For this steady flow, the first-order forward difference scheme is used for time stepping. The pressure contours captured is shown in figure 3(b), in which a detached shock wave is clearly displayed. The shock detector described in section 2 is used to obtain the shock point set, and only the pressure gradient is considered in this case. According to Eq.(1), the maximum cell gradient in the whole flow field and an appropriate threshold factor $k^s_{\text{thre},p}$ need to be defined. In the shock-capturing computation, the pressure gradient of the shock wave cell is affected by the grid scale and the slope limiter, and thus $k^s_{\text{thre},p}$ is given empirically, i.e.

$$k^s_{\text{thre},p} = 0.1.$$

Then, the cells whose pressure gradient ratio k_p are equal to or larger than the threshold factor $k^s_{\text{thre},p}$ are marked as shock cells, and their centers are recorded as shock wave points, as shown in figure 3(c). The shock wave captured by the shock-capturing method is a band of certain width. The proposed PRs method is used to fit this band into a shock surface in 3D or curve in 2D, for shock-fitting simulation.

The source point S is set at coordinates

$$(x_S, y_S) = (0.1, 0.0),$$

and the angle between two adjacent rays is taken as a constant

$$\varphi = 4.5^\circ.$$

In each subregion $A_i, i = 1 \cdots n-1$, the least-squares fitting method is used to fit the subset of shock points into a straight line. Finally, a series of feature points and one shock wave surface are obtained, as shown in figure 3(d). This surface is close to the shock front and can be conveniently used for shock-fitting simulation.

In the shock-fitting simulation, the extracted surface is used as a shock boundary where the flow variables are determined by the R-H relations. To improve the computation convergence, the initial flow variables are interpolated based on the shock-capturing solutions. To examine the advantage of this surface in the shock-fitting simulation, we chose three different surfaces as the shock boundary: the surface obtained by the PRs method and two random surfaces, as shown in figure 4.

The three grids have the same grid scale on the boundaries ($\Delta l = 0.001$), and their computation domains are composed of 8793, 6735 and 5875 nearly equilateral triangle cells, respectively, as shown in figure 5. Although the initial positions of the three shock waves are different, they eventually converge to the same status. The steady pressure contours and the maximum density residual convergence curves, as shown in figure 6 and figure 7, show that the converged pressure distributions are almost the same, but the Convergent rate are different. Better initial shock-fitting improves the convergence. Due to the significant error of the random surfaces the corresponding computations require more time steps to reach the converged results, causing large mesh deformation and even re-meshing. When the grid is re-meshed, interpolation is required to calculated the variables on the new cells, deteriorating the convergence. Using PRs method causes no re-meshing, but re-meshing happen at step 10000 in case Random 1, and at steps 400, 2200, 2800, 5000 and 10000 in case Random 2.

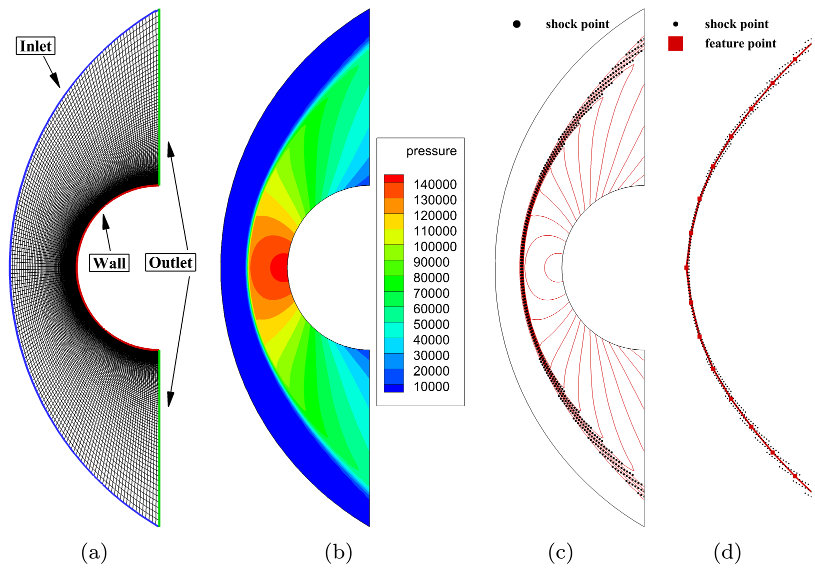

Figure 3: PRs method for detached shock in blunt body problem: (a) the computational mesh; (b) the pressure contours; (c) the locations of shock points ; (d) the feature points on shock surface.

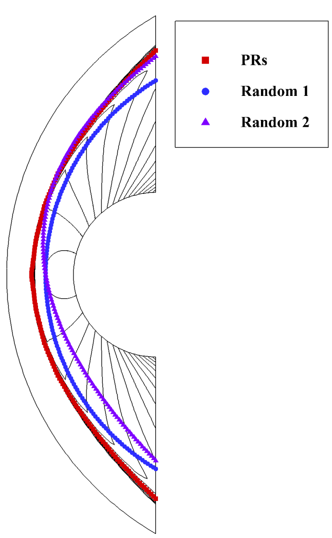

Figure 4: The location and shape of three different initial shock surfaces.

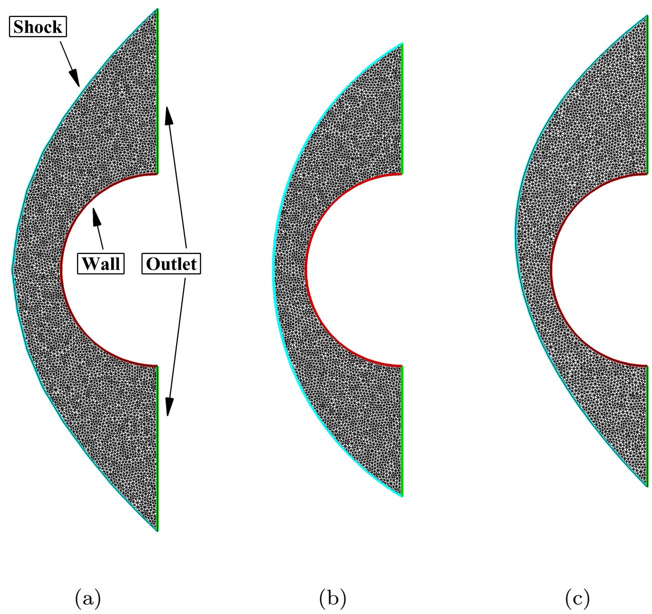

Figure 5: Three computation grids with using different initial shock surfaces for shock-fitting simulation: (a) PRs surface; (b) Random surface 1; (c) Random surface 2.

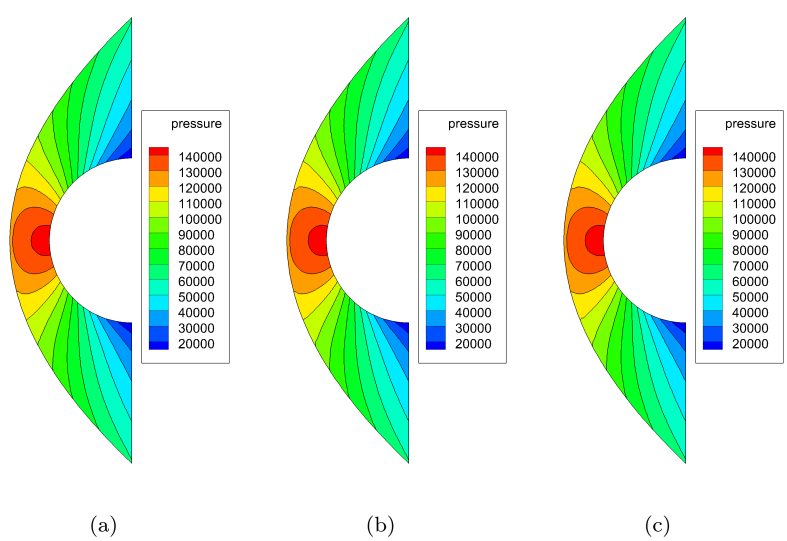

Figure 6: Steady pressure contours on various grids: (a) RPs; (b) Random 1; (c) Random 2.

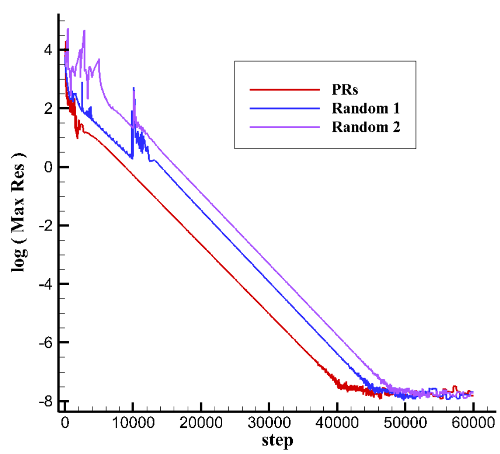

Figure 7: Convergent history of using different grids.

4.2 Shock reflection

In this section, a 2D shock reflection structure which contains reflection shock, Mach stem and contact discontinuity is presented. The surface extraction process of the shock and contact discontinuity is considered and the shock-fitting simulation is ignored since it has been detailed in another work [21].

The computational domain and boundary conditions are shown in figure 8, and the length of each edge is that $L_{AF} = 0.4$, $L_{AB} = 0.1$, $L_{DE} = 0.312$ and $L_{EF} = 0.85$, the angle between edge BC and edge AB is $\delta = 14.0°$. The boundary AF is a supersonic inlet, DE is a supersonic outlet and others are slip walls. The computational mesh grid is 300(rows) $\times$ 218(columns), the free-stream Mach number is $Ma = 1.9$ and the angel of attack is $\alpha = 0.0$.

An oblique shock wave that deflects the uniform upstream flow by angel δ is generated at point B, which will be denoted as *IS*. The incident shock wave *IS* is reflected on the wall *FE*, generating a Mach stem *MS*, a reflected shock *RS* and a contact discontinuity *SS*. The reflected shock *RS* is reflected again on the wall *CD*, resulting in a new reflected shock *RRS*. The above structures can be clearly described in the density contours, as shown in figure 9. In this case, taking into account the common features of contact discontinuities and shock waves, density gradient and pressure gradient are selected as detection indicators.

For shock waves, only the density gradient is considered, and the threshold factor is considered as

$$k^s_{\text{thre},\rho} = 0.03.$$

For contact discontinuity, the density and pressure threshold factors are considered as

$$k^c_{\text{thre},\rho} = 0.05 \quad and \quad k^c_{\text{thre},p} = 0.035.$$

Then, the shock points and contact discontinuity points can be recorded with using the detector described in section 2, as shown in figure 10. It is found that the detected point set has the same shape as the flow field structure. Because the shape of the point set is complex, it is difficult to fit it into a continuous curve in single step. Therefore, the piecewise fitting method will be applied. Firstly, set a source point S_1 in zone II, and the point subsets of incident shock *IS* and reflected shock *RS* will be fitted into a polyline by using the least-squares fitting method, in each subregion A_i, as shown in figure 11(a). Then, set the second source point S_2 in zone I to fit the subset of Mach stem *MS* into a curve. Due to the small number of *MS* points, it is not suitable to use the least-squares method for curve fitting in each subregion. Here, the average of the points within each subregion is directly used as the feature point, and the fitting result is shown in figure 11(b). Finally, set another source point S_3 in zone III, and the point subsets of contact discontinuity *SS* and reflected shock *RRS* will be fitted into two curves by using the least-squares fitting method in each subregion A_i, as shown in figure 11(c). It is worth noting that the sequence of setting these source points is not unique. Through this process, several curves matching the flow features are obtained, as shown in figure 12.

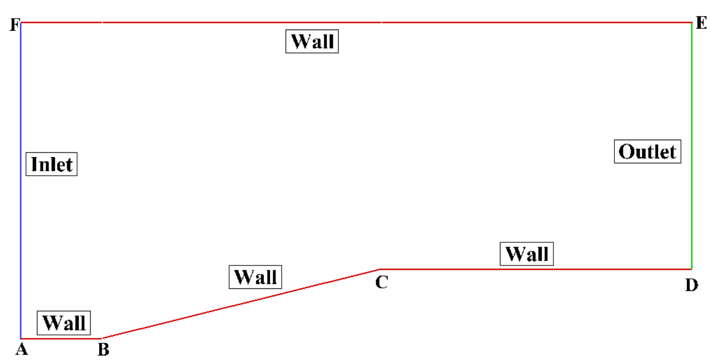

Figure 8: Shock reflection problem: computational domain.

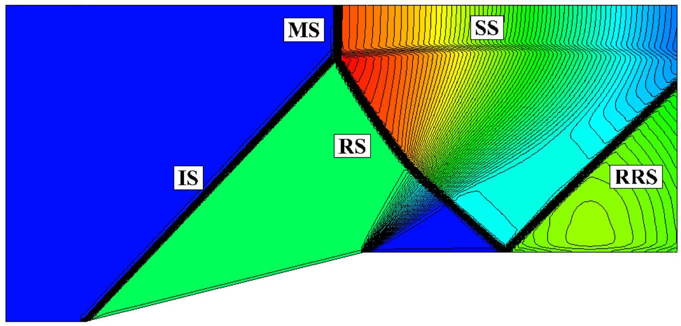

Figure 9: Shock reflection problem: density contours.

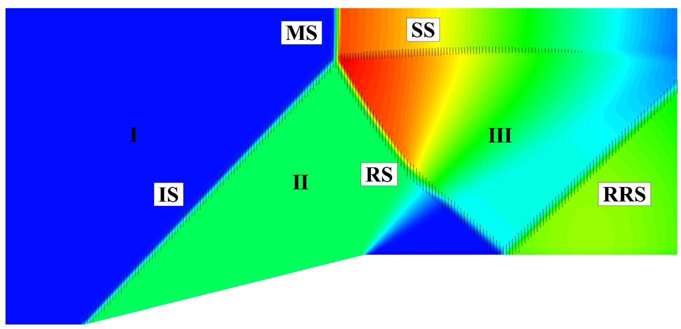

Figure 10: Shock reflection problem: discontinuities detection.

4.3 Blunt body problem in 3D

In this section, 3D blunt body supersonic flow problem is presented to test the performance of the PRs method in three-dimensional applications, but its shock-fitting simulation is also not discussed.

In this case, the free-stream Mach number is $Ma = 5.0$, the angle of attack $\alpha = 0.0$ and the sideslip angle $\beta = 0.0$. A hemisphere with a sphere center coordinate of $(0.0, 0.0, 0.0)$ and a diameter of $D = 0.0508$ is used as the computation model. The computation grid has 508365 hexahedral cells, as shown in figure 13.

The pressure contours is shown in figure 14, in which a clear shock wave can be found. In this case, the pressure gradient is selected as shock detection indicator, and the threshold factor is

$$k^s_{\text{thre},p} = 0.05.$$

The shock point set detected from flow field is shown in figure 15, and 23640 vertexes are marked. The thickness of the detected shock region is at least crossing three elements in the flow direction. The unit-sphere described in section 3.2 is used to fit this region into a surface. In this case, the unit-sphere has 1734 vertexes and 3464 triangular cells, as shown in figure 2(a). The centre of this sphere which represents the source point S is set at coordinates

$$(x_S, y_S, z_S) = (2.0, 0.0, 0.0).$$

The shock points in subregions determined by the rays emitted from the centre of the unit-sphere are fitted into triangular patches. These triangular patches ultimately define a shock surface which can be used in shock-fitting simulation directly, as shown in figure 16.

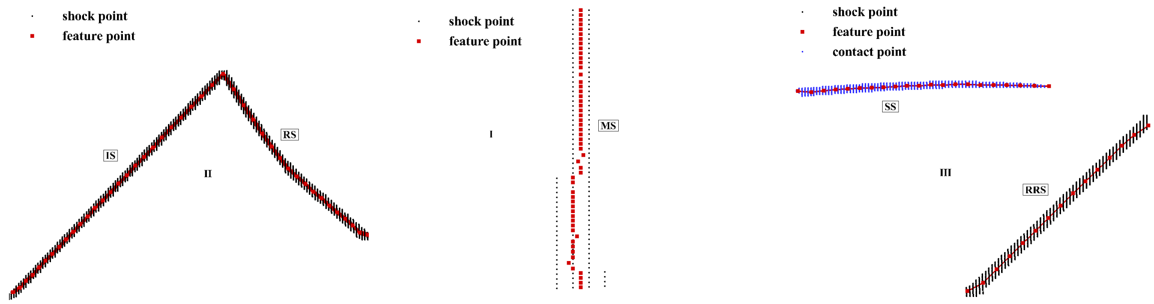

(a) (b) (c)

Figure 11: Shock reflection problem: PRs surface with piecewise fitting: (a) shock *IS* and shock *RS*; (b) Mach stem *MS*; (c) contact discontinuity *SS* and shock *RRS*.

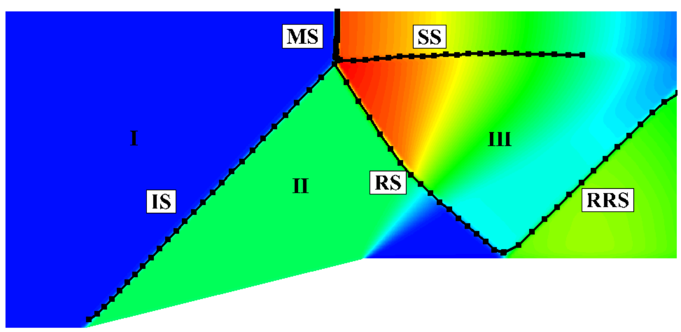

Figure 12: Shock reflection problem: discontinuity surfaces extracted by PRs method.

5 Conclusion

The shock wave detected in the flow field is usually not a shock surface but a shock region. The PRs method proposed in this paper can extract a shock surface from the shock region for the shock-fitting simulation. Especially for three-dimensional shock wave structures that are difficult to describe, this method provides a way to fit the initial shock waves. The results of the test cases show that the shock surface extracted by this method is consistent with the shock wave in the shock-capturing results. For the shock-fitting simulation of stationary shocks, if the initial shock surfaces are given, it usually takes several calculation iterations to make the shock boundaries and the internal flow field to converge to a steady state. For the simulation of transient shock, if the position or shape of the initial shock surface is inaccurate, uncorrectable errors may be introduced at the beginning of the computation. The present method provides a accurate initial shock surface for shock-fitting simulation, which effectively improves the computation efficiency and accuracy. In addition, this method is expected to provide a new tool for facilitating the local mesh refinement of grid-adaptation.

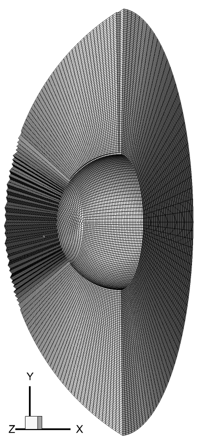

Figure 13: Computation mesh for 3D blunt body flow.

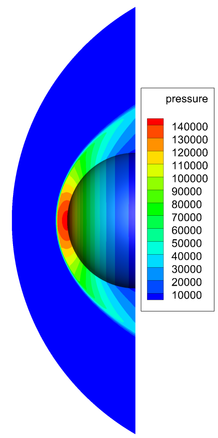

Figure 14: The pressure contours in 3D blunt body flow.

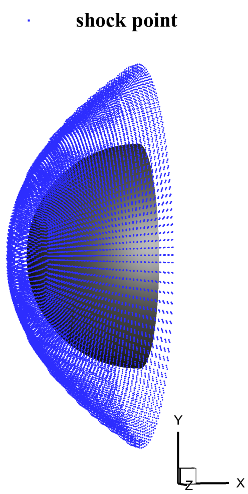

Figure 15: The shock point set in 3D blunt body flow.

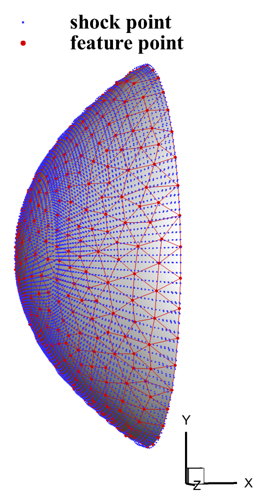

Figure 16: The extracted shock surface with using PRs method in 3D blunt body flow.

Acknowledgements

This work is partially supported by National Natural Science Foundation of China under the grants of 91541117 and 11532016.

References

[1] P.D. Lax. Weak solutions of nonlinear hyperbolic equations and their numerical computation. *Communications on pure and applied mathematics*, 7(1):159–193, 1954.

[2] P.D. Lax and B. Wendroff. Systems of conservation laws. *Communications on Pure and Applied mathematics*, 13(2):217–237, 1960.

[3] A. Harten. High resolution schemes for hyperbolic conservation laws. *Journal of computational physics*, 49(3):357–393, 1983.

[4] H. Zhang. Non-oscillatory and non-free-parameter dissipation difference scheme. *Acta Aerodynamica Sinica*, 2:143–165, 1988.

[5] C. Shu and S. Osher. Efficient implementation of essentially non-oscillatory shock-capturing schemes. *Journal of computational physics*, 77(2):439–471, 1988.
[6] X. Liu, S. Osher, and T. Chan. Weighted essentially non-oscillatory schemes. *Journal of Computational Physics*, 115(1):200–212, 1994.
[7] J. VonNeumann and R.D. Richtmyer. A method for the numerical calculation of hydrodynamic shocks. *Journal of Applied Physics*, 21(3):232–237, 1950.
[8] P.K. Kundu. *Fluid Mechanics.* ACADEMIC PRESS, 1990.
[9] Q. Wu and W. Chen. *Rarefied gas dynamics.* National University of Defense Technology Press, 2004.
[10] G. Moretti and M. Abbett. A time-dependent computaional method for blunt body flows. *Aiaa Journal*, 4(5):736–741, 1966.
[11] G. Moretti. Thirty-six years of shock fitting. *Computers \& Fluids*, 31(4-7):719–723, 2002.
[12] D. Zhang. *A Course in Computational Fluid Dynamics.* HIGHER EDUCATION PRESS, 2010.
[13] R.D. Robert and K.W. Morton. *Difference Methods for Initial-Value Problems.* Interscience Publishers, 1967.
[14] M.D. Salas. Shock fitting method for complicated two-dimensional supersonic flows. *Aiaa Journal*, 14(5):583–588, 1976.
[15] P.S. Rawat and X. Zhong. On high-order shock-fitting and front-tracking schemes for numerical simulation of shock-disturbance interactions. *Journal of Computational Physics*, 229(19):6744–6780, 2010.
[16] A. Prakash, N. Parsons, X. Wang, and X. Zhong. High-order shock-fitting methods for direct numerical simulation of hypersonic flow with chemical and thermal nonequilibrium. *Journal of Computational Physics*, 230(23):8474–8507, 2011.
[17] R. Paciorri and A. Bonfiglioli. A shock-fitting technique for 2d unstructured grids. *Computers \& Fluids*, 38(3):715–726, 2009.
[18] R. Paciorri and A. Bonfiglioli. Shock interaction computations on unstructured, two-dimensional grids using a shock-fitting technique. *Journal of Computational Physics*, 230(8):3155–3177, 2011.
[19] J. Liu, D. Zou, and C. Xu. An unsteady shock-fitting technique based on unstructured moving grids. *ACTA AERODYNAMICA SINICA*, 33(01):10–16, 2015.
[20] J. Liu, C. Xu, and X. Bai. *Finite volume methods and unstructured dynamic meshes.* Science Press, 2016.
[21] D. Zou, C. Xu, H. Dong, and J. Liu. A shock-fitting technique for cell-centered finite volume methods on unstructured dynamic meshes. *Journal of Computational Physics*, 345:866–882, 2017.
[22] J. Liu, D. Zou, and H. Dong. A moving discontinuity fitting technique to simulate shock waves impinged on a straight wall. *Acta Aeronautica et Astronautica Sinica*, 37(03):836–846, 2016.
[23] J. Liu, D. Zou, and H. Dong. Principle of new discontinuity fitting technique based on unstructured moving grid. *Physics of Gases*, 2(01):13–20, 2017.
[24] H.G. Pagendarm and B. Seitz. An algorithm for detection and visualization of discontinuities in scientific data fields applied to flow data with shock waves. In *P. Palamidese (ed.): Ellis Horwood Workshop," Scientific Visualization, Advance Software Techniques", 1993*, pages 161–177. Ellis Horwood Limitid, UK, 1993.
[25] D. Lovely and R.Haimes. Shock detection from computational fluid dynamics results. In *14th Computational Fluid Dynamics Conference*, page 3285, 1999.
[26] M. Kanamori and K. Suzuki. Shock wave detection in two-dimensional flow based on the theory of characteristics from cfd data. *Journal of Computational Physics*, 230(8):3085–3092, 2011.
[27] M. Kanamori and K. Suzuki. Shock wave detection based on the theory of characteristics for cfd results. In *20th AIAA Computational Fluid Dynamics Conference*, page 3681, 2011.
[28] M. Abbett and G. Moretti. A time-dependent computational method for blunt body flows. *AIAA Journal*, 4(12):2136–2141, 1966.
[29] A.N. Lyubimov and V.V. Rusanov. *Gas Flows Past Blunt Bodies. Pt. 2. Tables of the Gasdynamic Functions.* NASA, 1973.
[30] Fan Zhang, Jun Liu, and Biaosong Chen. Modified multi-dimensional limiting process with enhanced shock stability on unstructured grids. *Computers & Fluids*, 161:171 – 188, 2018.